Electron Capture Heating in the Neutron Star Crust

Dr. Sanjib S. Gupta, Dept. of Physics, IIT-Ropar

Nuclear reactions in the crust of a neutron star (NS) form an important bridge between the extensively studied nuclear burning on the surface and the less well understood neutrino cooling processes in the core, where exotic states of matter can exist. Observation of accreting neutron stars in binary systems is proving to be a promising new tool to probe the thermal evolution of the inner core and its neutrino cooling rate. In particular, the ignition of "X-ray super bursts" (XRSB) due to ^{12}C fusion has been shown to be sensitive to the thermal profile of the neutron star crust[1]. Similarly, neutron stars exhibiting intermittent periods of rapid accretion ("transients") have a quiescent luminosity which is thought to be powered by the heat released in the crust[2].

Surface burning on an accreting NS by the "rp-process" (rapid proton capture) in a Type-I X-ray Burst(XRB) [3,4] produces heavy elements near the proton drip-line. As these ashes are buried by subsequent accretion successive electron capture(EC) reactions occur as the electron chemical potential EF increases rapidly with depth. In pioneering work a decade ago, Haensel and Zdunik outlined these EC reactions in a one-component plasma(OCP) and found that the heat released in EC was not substantial –most of the energy release occurred much deeper in the crust through pycnonuclear fusion reactions[5,6]. More recently in a multi-component plasma(MCP) simulation, Gupta et.al. found that EC to excited states and subsequent γ-de excitation increased the heating at shallow depths [7]. In this paper we report that EC captures to highly excited daughter states also lead to neutron emission processes near the neutron drip-line that are vastly accelerated when the level schemes of deformed neutron-rich nuclei are incorporated as opposed to when emissions are restricted to ground states(g.s.). These reactions fundamentally change the direction and speed of the reaction pathway and alter the crustal heating profile.

For $E_F \sim 27$ MeV there will be a neutron chemical potential $\mu_n > 0$ and consequently a free neutron abundance. The depth $E_F \simeq 27$ MeV is called the "neutron drip" (ND) point. Close to ND ($E_F \sim 25$ MeV), EC can occur into excited states with $E_{exc} > S_{xn}$ where S_{xn} is the separation energy for x neutrons. These reactions are henceforth referred to as (EC, xn) reactions. Once (EC, xn) is allowed at $E_F \sim 25$ MeV, any EC is always accompanied by some neutron emission since the $x > 3$ channels are always open and the $x = 0$ channel("pureEC") is highly suppressed. Post-ND the products of (EC,xn) can be highly EC-unstable("superthreshold") at $(Z-1)$ since the neutron number N has also been substantially lowered. Although some of these nuclei will recapture neutrons, yet the favored N after (n,γ) will not be as high as the pure EC pathway would have permitted, due to the powerful non-thermal driving force removing neutrons. This force is $(E_F - E_{thresh\ ,g.s.} - S_{xn})$ and since it is much greater than kT the superthreshold (EC,xn) rates are also independent of temperature. The temperature can only drive neutron emission for $S_n \sim 1.4$ MeV by (γ,n). Consequently, the density-driven (EC,xn) rates, which are more than a factor of 10^6 larger than the (γ,n) rates, expand the path into a band $1.0\ \text{MeV} \leq S_n \leq 3.5$ MeV. Nuclei in this band are generally EC-unstable at $EF > 5$ MeV. Hence, each of the (EC,xn) products (resultant network nodes

for different x) are subjected to reaction-driving energies (EF $-E_{thresh,g.s.} - S_{xn}$)that can be higher than in the previous (EC,xn) reaction step, leading to a dense web of subsequent(EC,xn) branching or a "Superthreshold(EC,xn) Cascade" (henceforth called the SEC-process) rapidly lowering both (Z) and (A). For clarity, we denote the absolute value of the g.s. nuclear mass differences as $E_{thresh,g.s.}$ while an actually encountered threshold is always written as E_{thresh} and includes the energy of the first state to which EC is allowed, which may not be the g.s. Our network includes EC (β^+) and β^- rates from the proton drip-line to the neutron drip - line using transition matrix elements from the QRPA model described in [8]. Calculated values of deformations from [9] were consistently incorporated for Z > 8 nuclei , below which we have assumed a typical quadrupole deformation $\varrho 2$ =0.55. From any excitation energy E_{exc} in the EC daughter (Z−1,A)the neutron decay and competing γ-ray emission branching ratios are calculated with the nuclear reaction code GNASH [10]. This code employs the statistical Hauser-Feshbach (HF) method augmented with a Direct-Semi-Direct (DSD) component [11] for those nuclei in which the direct reactions will dominate. The maximum excitation energy considered is 30MeV, and upto 20 emitted neutrons are allowed. We account for neutron kinetic energies which reduce the available energy for subsequent neutron emissions. For Z < 10 we do not use HF or DSD for the neutron branches: rather, if EC occurs into a state above S_{xn} but below $S_{(x+1)n}$, then the x-neutron branch is given full strength and all others are set to zero.

We use radiative neutron capture (n,γ) rates from [12]. The reverse (γ,n) rate for a typical pre-ND crust nucleus ^{105}Kr (ignoring partition functions) is $\lambda=(N_A(\sigma v)Y_n)\times 10^{10} \times T^{1.5} \exp(-11.605S_n/T9) = 7.82 \times 10^{-13}$ s which is already too slow to compete with the accretion timescale $\Delta t \sim 10^9$ s during which the resulting ΔEF can make(EC,xn) reactions competitive. Typically, only nuclei with $S_n < 1.4$ MeV have (γ,n) competitive with accretion at T ~0.5 GK. The products of these (γ,n) are susceptible to EC which produce (Z −1) nuclei, and the process continues to lower A by further(γ,n). In models that rely on the stellar photon bath to produce neutrons by (γ,n) reactions, this will be a valid path way pre-ND(but constrained by $S_n \sim 1.4$MeV). In the vicinity of ND ($E_F \sim 25$ MeV), however, the (EC,xn) rates are more than a factor of 10^6 larger than the (γ,n) rates. Also,from a heating efficiency perspective, the slow pre-ND(γ,n) reactions have a negligible effect –beyond EF ~ 25MeV the SEC-process removes any residual compositional memory. Furthermore, at $E_F \sim 20$ MeV the number density of thermal photons is suppressed because the propagating photon is dressed in the medium (the dressed particle is called the plasmon) and acquires a finite mass ≈ 1.3 MeV at $\rho Ye \sim 10^{11}$ g/cc increasing to about 4.1 MeV at 10^{12} g/cc. Here Ye, Ne, me are electron fraction, number density and rest mass, respectively. Under typical conditions in the crust (10^{11} g/cc, 0.5 GK) the number density of photons is suppressed by the factor $\exp(-\hbar\omega_p/kT)$. At $\hbar\omega_p \sim S_n \sim 1.4$ MeV, this suppression has a strong effect $\simeq 10^{-13}$ at energies important to the pre-ND (γ,n) reactions. Furthermore, the Plasmon suppression increases with increasing density: $\exp(-\hbar\omega_p/kT) \simeq 10^{-42}$ at 10^{12} g/cc and 0.5GK.However, the higher the electron density ,the more efficient the(EC,xn) processes become at removing neutrons from increasingly higher excitation energies. Furthermore, the high Nuclear Level Densities (NLDs) at $E_{exc} \sim S_{xn}$ and the high superthreshold phase–space factors involved ensure that the SEC-process is a robust mechanism with negligible sensitivity to uncertainties in the underlying nuclear model. The (EC,xn) timescales will always be shorter than the accretion and the (γ,n) timescales by several orders of magnitude in a global nuclear model used to calculate the EC

daughter excitation energies. The speed of the resulting reaction flow will be unaffected by the choice of global nuclear model, though the "transit points" at a given E_F may differ slightly. We highlight two aspects of the QRPA model we have used which have significant global impact:(1) the single-particle model serving as input to the QRPA is a complete model space (no levels will be systematically missing) and (2) we treat deformation realistically. Though global Shell Model calculations of weak interaction strengths for the heavy and/or neutron–rich

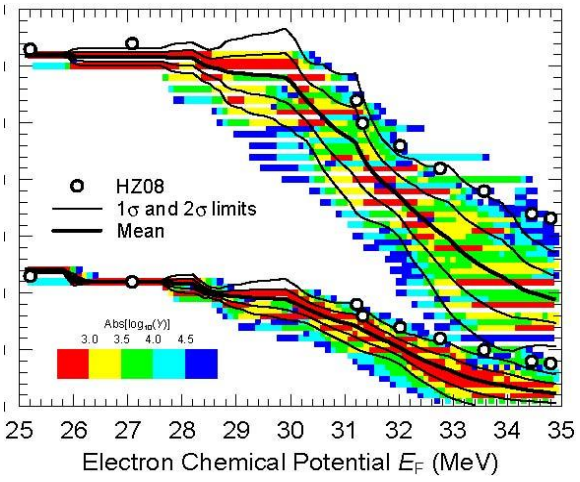

FIG.1*: Abundance distributions Y(N)and Y(Z)shown for abs(log_{10}(Y))< 5at ΔE_F =0.1 intervals in the E_F range 25–35 MeV for an MCP calculation starting with pure ^{106}Pd. Beyond EF ~ 26 the MCP distributions of Y(N)and Y(Z) rapidly broaden due to EC into highly excited states followed by neutron emissions. The OCP trajectories of [13] starting with the same ICC and evolving through EC and g.s. neutron emissions lie outside the 2σ limits of the MCP Y(N) and Y(Z) distributions.*

nuclei of interest are simply not available, the same considerations of high NLD at high E_{exc} apply to nuclear structure computed in the Shell Model as they do to the QRPA calculations.

The combined effects of g.s. to g.s. EC and g.s. neutron emissions in the crust was referred to as the "inverse r-process" by [14]. However, the possibility of "superthreshold" (EC,xn), with very large driving forces that lead to further cascades within an arrow ΔEF slice of the crust was not explored. In fact, since earlier models had neutron emission only from g.s. they missed important nuclear structure effects in deformed neutron-rich nuclei. The level spacings in these exotic nuclei can influence flows by changing (EC,xn) rates and branchings with only a small change in E_F. Moreover, (1) the SEC-process is quite distinct from the r-process in the Waiting Point Approximation where at a certain temperature(n,γ)−(γ,n) equilibrium along constant Z occurs since the (EC,xn) "reverse rate" is more than a factor of 10^6 larger than the (γ,n) rate (even without plasmon suppression);(2) the (EC,xn) rate increases with proton-richness, unlike the (γ,n) rate in the r-process; and (3) the non-thermal reaction energy source E_F is not even approximately constant, as it increases steadily with depth in the NS crust Therefore, there are few similarities with the r-process, except that the SEC-process runs in the opposite direction in the ZN-plane. Since the SEC-process covers wide ranges of the nuclear chart with a dense web of competing(EC,xn) channels, it becomes difficult to identify individual nuclei that play a dominant role at a given EF once the r.m.s deviation ΔN. increases to > 5 for the abundance distribution Y(N). Rather, we plot the means (N)and (Z) and the r.m.s. deviations ΔZ, ΔN (and also 2ΔN and 2ΔZ) of the abundance distributions Y(N) and Y(Z) with changing E_F in fig.1 to compare our MCP evolution with the OCP evolution of [13]starting with the same initial crust composition(ICC) of pure ^{106}Pd. We start the evolution at EF ~ 0.5MeV (ρ ~ 10^6 g/cc) and terminate our simulation when fusion reactions begin to cycle material out of the Z ~ 10 region at EF ~ 38 MeV (ρ ~ $10^{12.5}$ g/cc). Prior to neutron emission the "pure EC" path through even-even nuclei is the same as in the OCP calculation of [13]:

^{106}Pd→ ^{106}Ru→ ^{106}Mo→ ^{106}Zr→ ^{106}Sr→ ^{106}Kr→ ^{106}Se. However, ^{106}Se→ ^{106}As at E_F =25.86 MeV is to E_{exc} =2.45 MeV > S_{3n} = 0.99 MeV and neutron removal can produce nuclei up to ^{103}As. Now E_{thresh} =23.46, 24.44, 24.12MeV for respectively allowed "superthreshold" (EC,xn) branching with high values of x. Thus, (N) begins a rapid descent and the MCP trajectory does not produce N =74 at ^{106}Ge accessed at EF ≃ 27 MeV in the OCP(fig.1). Well–deformed ^{106}As (ϱ2 =0.225from[9]) has neutron energy levels spaced by a few 100keV, each participating in (EC,xn) over a very small change ΔE_F in E_F. This effect combined with a low S_n results in multiple neutron emission towards (spherical) sub shell closures at N = 64,56. Hence, ΔN suddenly expands to ∼ 5 beyond the sub shell N =70 and the slope of (N) abruptly changes as neutrons are rapidly emitted between N =66 and56.We follow the increasingly dense web of (EC,xn) branching from ^{103}As(EC,1n)^{102}Ge onwards. The product undergoes upto (EC,3n) at E_F ∼ 28 MeV. A dominant branch at 53% is to ^{101}Ga whose (EC,xn) products are $^{100-98}$Zn, each with branchings between 30 and 40%.The flow is now no longer concentrated along a single x-neutron emission channel. At E_{thresh} = 28.6 MeV ^{98}Zn(EC,xn) occurs with x ≤ 3. The product ^{95}Cu (= 66) has E_{thresh} = 28.8 MeV and releases up to 6 neutrons with substantial branching ratios. Due to this rapidly expanding web of (EC,xn) with increasing x, neutrons are emitted continuously as E_F rises, and consequently at E_F ≃ 29 MeV(fig.1) flow from N = 66 to N = 60 is already at the factor of 3 level by abundance. In contrast, the OCP essentially does not evolve from E_F = 27.08 up to 31.22 MeV, i.e. there is no activity between production of ^{106}Ge and its destruction by ^{106}Ge+4e$^-$ → ^{92}Ni+14n+4ν_e (and there is a huge gap of 4.14 MeV between the productions of ^{106}Ge and ^{92}Ni). In contrast, the MCP neutron emission is much more continuous with changing E_F. At higher E_F in the MCP evolution, fig.1 clearly shows that within the (spherical) neutron g9/2 sub shell (N between 40 and 50) there are several transit points in N that become accessible at very closely spaced E_F. These correspond to the well-separated deformed neutron levels emanating from the same (spherical) subshell. A level diagram of mid-proton-shell ^{80}Cr(deformed with ϱ2 =0.233) not only shows this effect, but also that upon entry into the N =56 subshell closure, N =54,52 should play a prominent role and N = 52,50 correspond to levels at almost identical energy. Therefore, the MCP N-evolution flattens at N = 56 and 40, but not at N = 50, through which it is rather steep. Throughout the evolution the OCP slope of N(EF) (with notable exceptions at N = 64,60 corresponding to Z = 28,26) is closer to the MCP slopes of (N)(±2ΔN) between major neutron(sub)shells (see the MCP slopes at N = 56,40 in fig.1)–thus the OCP g.s. neutron removals do not reflect the rich structure within neutron(sub)shells for well-deformed neutron-rich nuclei.

This scenario is highly unlikely if (1) neutron emissions occur from excited states – instead of the typical(2EC,6n) steps of the OCP evolution at widely separated EF,(EC,xn) with much higher x can participate in the MCP at several closely spaced EF, and (2) there is more than one network node so that 100% of the flow is not controlled by a single x ≈ 3 neutron emission mode like a typical OCP(2EC,6n) on ^{80}Cr at EF = 32.76 MeV. If we remove only 3 neutrons after the threshold capture on ^{80}Cr, the product ^{77}Vis still superthreshold to(EC,xn) by almost 4 MeV. The MCP branchings $\gtrsim$ 10% on the ^{77}V intermediate nucleus are 12.6%(EC,4n), 38.4%(EC,5n), 15.8%(EC,6n), 19.2%(EC,7n) showing odd-even and neutron kinetic energy subtraction effects. The resulting large spreads ΔN,ΔZ in the MCP evolution allow much smoother movement through several MCP

network nodes. This occurs because any one of the network nodes(Z−1,N +1),(Z−1,N),(Z−1,N −1),... resulting from different x in a single(EC,xn) step can itself move on to lower N and Z through(EC,xn) either at the prevailing E_F or with a small increase $\Delta E_F \sim 0.3$ MeV. The nuclear structure probed by the high energy (EF − Ethresh) of "superthreshold (EC,xn)" determines the characteristics of the reaction flow in the following ways:

(1)The slopes of (N),(Z) with E_F, or the speed of the reaction flow, comes from a removal of the (spherical) subshell degeneracy due to deformation. This effect is strongest midway between spherical (sub)shells. The OCP curve passes through N = 64, 60, 56,52,48,44,40,36,30 with large gaps $\Delta E_F \sim 1$ (and a huge gap of 4.14 MeV between the productions of ^{106}Ge and ^{92}Ni).In contrast, the MCP neutron emission is much more continuous with changing E_F. At higher E_F in the MCP evolution, fig.1 clearly shows that within the(spherical) neutron g9/2 subshell (N between 40 and 50) there are several transit points in N that become accessible at very closely spaced E_F. These correspond to the well-separated deformed neutron levels emanating from the same (spherical) subshell. A level diagram of mid-proton-shell ^{80}Cr(deformed with $\varrho 2$ =0.233) not only shows this effect, but also that upon entry into the N =56 subshell closure, N =54,52 should play a prominent role and N = 52,50 correspond to levels at almost identical energy. Therefore, the MCP N-evolution flattens at N = 56 and 40, but not at N = 50, through which it is rather steep. Throughout the evolution the OCP slope of $N(E_F)$(with notable exceptions at N = 64,60 corresponding to Z = 28,26) is closer to the MCP slopes of (N)($\pm 2\Delta$N) between major neutron(sub)shells (see the MCP slopes at N = 56,40in fig.1)–thus the OCP g.s. neutron removals do not reflect the rich structure within neutron(sub) shells for well-deformed neutron-rich nuclei.

(2)ΔN and ΔZ increase to reflect the occupancies of accessible(sub)shells at a given E_F. An example is the increase of ΔN to (40−28)/2 = 6 closely matching the network value of 6.44 at E_F =33.5 MeV. Levels beneath subshell closures at N =38,32 are all accessible at this E_F but N between 28 and 20 is only accessed at N =26 by highly abundant nuclei.

(3)Unlike the OCP evolution, branchings populate odd-A chains also – these are rapidly depleted, driving abundance to lower Z faster.

(4)The free neutron abundance X_n increases smoothly with EF due to the large number of available (EC,xn) sources at each depth in marked contrast to the discontinuous evolution of $X_n(E_F)$in the OCP (see[5, 6, 13]).

The resulting distribution Y(N) at any EF is multiple-peaked primarily due to odd-even and neutron(sub)shell effects. It is also highly asymmetric with long neutron-deficient tails that are susceptible to further (EC,xn). This leads to a broadening of Y (Z) to the extent allowed by the accessible proton (sub)shells.

Beyond $E_F \sim 29$ MeV the MCP rapidly diverges from the OCP since roughly $[(2\Delta Z) \times (2\Delta N)] \approx 5\times 10 = 50$ network nodes are simultaneously processing the abundances unlike a single node in an OCP scenario. This dense Markov process of (EC,xn)transitions (1)quickly removes compositional memory of the XRB ashes through several N-nodes at each Z (and vice-versa), which is not possible in an OCP evolution, and (2) changes the evolutionary description from one of individual nuclei at specific E_F (which is possible for the OCP) into that of r.m.s. deviations and higher moments which ultimately determine the shapes of the Y(N) and Y(Z)distributions. These shapes are clearly discernible in fig.1 since the color changes denote abundance variations by a factor of only $10^{0.5} \simeq 3$. The large spreads ΔN and ΔZ in these distributions are important inputs to

models of transport processes in the crust such as those determining thermal conductivity.

The efficiency of the SEC-process in heating the crust is shown in fig.2.We have the remarkable result that MCP crustal heating profiles from two very different ICC from possible Superburst progenitors change slope drastically near EF ∼ 35 MeV and converge to within ∼ 0.1 MeV/u of each other. This is of the order of the difference in BE/A of the ICC. Note that the MCP heating diverges from the OCP at a depth $E_F \simeq 30$ MeV where the MCP slopes of (N)(±2ΔN) change dramatically in fig.1.

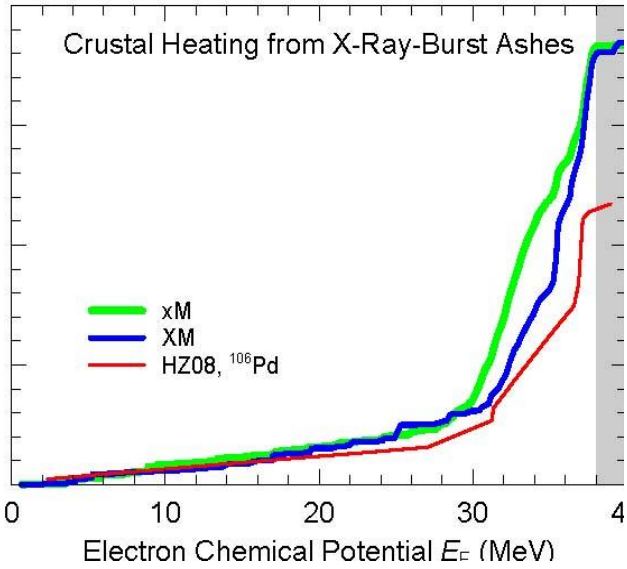

FIG.2*: Crustal heating in our MCP model for ICC (XRB ashes from[3]) from NS accreting 5% solar(x) and solar metallicities(X) at the accretion rate M = 0.1 ˙characteristic of Superburst progenitors (accretion at the Eddington limit is ˙mEdd ≈ 8.85· 10*^{4} *gcms*$^{-1}$*). Also plotted are OCP heating from [13] for the ICC comprised of* ^{106}*Pd. ICC from multizone XRB model xM : Peak A ∼ 100 −110 (very similar to the 1-zone rp-process products of [4] and also to an ICC of pure* ^{106}*Pd in the OCP model of [13]). ICC from model XM is a bimodal abundance distribution with significant pre-Fe-peak abundance, and also in A ∼60−80.*

The bulk of deep crustal heating by the SEC-process occurs in a narrow region post-ND, rather than near the crust-core interface if pycnonuclear fusion dominates. Being further from the core this new crustal heating mechanism can result in thermal profiles conducive to the ^{12}C ignition of X-ray Superbursts. Furthermore, unless the ICC is comprised only of pre-Fe-peak nuclei concentrated in A = 36−44(fig.7 of[7] explains why shallow heating should differ in this case; however the total crust heating will still differ by < 0.2MeV/u from MCP evolution of other ICC), the composition as a function of depth is not dependent on the ICC. Thus for a large class of accreting NS, the composition-dependent conductivities and crust neutrino cooling will look very similar, and so will the crustal thermal profiles which depend on these quantities.

[1] E. F. Brown, Astrophys. J. 614, L57(2004).

[2] E.F. Brown, L. Bildsten, and R. E. Rutledge, Astrophys. J. 504, L95(1998).

[3] S.E.Woosley et. al., Astrophys. J. Supp. Ser. 151, 75(2004).

[4] H.Schatz et al., Phys. Rev. Lett. 86, 3471(2001).

[5] P. Haensel and J. L. Zdunik, Astron. & Astrophys. 227, 431(1990).

[6] P. Haensel and J. L. Zdunik, Astron. & Astrophys. 404, L33(2003).

[7] S. Gupta et. al., Astrophys. J. 662, 1188(2007).

[8] P. Moller and J. Randrup, Nuc. Phys. A 514, 1(1990).

[9] P. Moller, J. R. Nix, W. D. Myers, and W. J. Swiatecki, ADNDT 59, 185(1995).

[10] P. Young, E. Arthur, and M. Chadwick, LA-12343-MS, Los Alamos National Laboratory (1992).

[11] L. Bonneau, T. Kawano, T. Watanabe, and S. Chiba, Phys. Rev. C 75, 054618(2007).

[12] T. Rauscher and F.-K. Thielemann, ADNDT75, 1(2000).

[*13] P. Haenseland J. L. Zdunik, Astron. & Astrophys.

480, 459(2008).

[14] K. Sato, Prog. Theor. Phys.62, 957(1979).